Preprints of the 21st IFAC World Congress (Virtual)
Berlin, Germany, July 12-17, 2020

Wind Tunnel Testing of an Optimal Feedback/feedfoward Control Law for Wind Turbines ⋆

Michael Sinner * **Vlaho Petrović** ** **Frederik Berger** **
Lars Neuhaus ** **Martin Kühn** ** **Lucy Y. Pao** *

* *Department of Electrical, Computer, and Energy Engineering, University of Colorado, Boulder, CO 80309 USA (e-mail: michael.sinner@colorado.edu, pao@colorado.edu).*
** *ForWind – Center for Wind Energy Research, Institute of Physics, University of Oldenburg, Oldenburg, Germany (e-mail: vlaho.petrovic@uol.de, frederik.berger@uol.de, lars.neuhaus@uol.de, martin.kuehn@uol.de)*

Abstract: With the development of lidar technology for measuring wind disturbances ahead of a wind turbine, various feedforward control techniques have been proposed to utilize preview disturbance information for rotor speed regulation. Among these is model predictive control (MPC), which generates an optimal control trajectory subject to system constraints, but very few physical tests have been conducted using MPC for wind turbines presumably due to the challenges involved in solving an optimization problem online. In this paper, we test an optimal feedback/feedforward control algorithm that maintains the clear disturbance inclusion of MPC but results in a linear control law that can be implemented easily. On the other hand, the proposed controller is not able to handle physical system constraints explicitly—full MPC is the subject of future work. A scaled wind turbine model in a wind tunnel is used for testing.

Keywords: linear optimal control, feedforward control, control applications, wind turbines, wind energy, integral action, time delay

1. INTRODUCTION

The inclusion of preview disturbance information in wind turbine control systems has been a topic of significant interest since it was suggested by Harris et al. (2005) and field tested by a research group led by the National Renewable Energy Laboratory (NREL) and the University of Stuttgart in the early 2010s (Scholbrock et al., 2013; Schlipf et al., 2014; Haizmann et al., 2015; Schlipf et al., 2015). The majority of research focuses on the use of lidar to produce an estimate of the incoming wind field by measuring the Doppler shift produced as light from a laser beam is backscattered by aerosols in the approaching wind. This estimate can be used by feedforward controllers to anticipate disturbance events and actuate accordingly, reducing the disturbance's impact at the turbine rotor.

The power production of a wind turbine is usually split into two regions categorized by below-rated and above-rated winds. In below-rated conditions, the control objective is to maximize the power produced. In this operation, the pitch angle of the turbine blades is kept constant while the rotor speed is varied to maximize power extraction using generator torque control (Pao and Johnson, 2011). On the other hand, in above-rated conditions the goal is to minimize structural loading on the turbine components while maintaining 'rated' power production. This can be achieved by keeping a constant generator torque and pitching the blades to vary the lift generated and regulate the rotor speed to its rated value. For a tutorial description of wind turbine control, we refer the reader to Pao and Johnson (2011). Studies have found that the use of feedforward information is more effective for regulating rotor speed in above-rated conditions than for power maximization in below-rated winds (Spencer et al., 2012; Scholbrock et al., 2016). We therefore consider only rotor speed regulation (e.g. Schlipf and Kühn, 2008; Dunne et al., 2011; Scholbrock et al., 2013) in this work.

Recently, optimal control techniques such as model predictive control (MPC) have been considered for wind turbine control (Schlipf et al., 2013; Jain et al., 2015; Mirzaei and Hansen, 2016; Gros and Schild, 2017). MPC has gained research attention for its straightforward inclusion of preview disturbance measurements and ability to handle system constraints; however, MPC generally involves solving an optimization problem online, and physical tests of MPC are scarce. In this work, we present a linear-quadratic regulator-like optimal control problem that retains the disturbance inclusion capabilities of MPC, while resulting in a feedback/feedforward control law that is linear. We demonstrate the controller with wind tunnel testing on a

⋆ This work was supported in part by Envision Energy, the German Academic Exchange Service (DAAD), the Hanse-Wissenschaftskolleg in Delmenhorst, Germany, and a Palmer Endowed Chair at the University of Colorado Boulder. The wind tunnel campaign, the active grid, and MoWiTO were supported by the German state of Lower Saxony within the project "ventus efficiens".

scaled turbine model. In future work, we plan to extend this work to constrained MPC, which involves implementing an online solver.

This paper is laid out as follows. Section 2 discusses several wind turbine models used in this study. Section 3 provides a derivation of the optimal feedback/feedforward control law. Section 4 describes the physical test bed and preview filter used. Section 5 presents the results of simulation and experimental wind tunnel testing. Section 6 comments on the results and motivates further work.

2. MODELING

2.1 Scaled Wind Turbine Model

Wind turbines are flexible structures that combine principles from elastic structures with aerodynamics and exhibit inherently nonlinear behavior. The ForWind Model Wind Turbine Oldenburg (MoWiTO) is a fully-actuated (individual blade pitch and generator torque) 1.8 m rotor-diameter turbine designed as a scaled model of the NREL 5MW reference turbine (Jonkman et al., 2009). For details on MoWiTO, see Berger et al. (2018).

2.2 FAST Model

We use an aero-elastic model of MoWiTO implemented in FAST v8 (full description of earlier version: Jonkman and Buhl Jr., 2005; change guide for version 8: Jonkman and Jonkman, 2016) for simulation and controller validation purposes. FAST allows turbine designers to model the complex nonlinear response of the turbine over a range of conditions from simple uniform, constant winds to highly turbulent, spatially- and temporally-varying wind fields. The FAST model is embedded in a Simulink environment for simple controller implementation and tuning.

2.3 Linear Time-invariant Model

For the purpose of linear-quadratic regulation with disturbance preview, we require a discrete-time state-space model of the plant

$$x_{k+1} = Ax_k + Bu_k + B_d d_k \tag{1a}$$
$$y_k = Cx_k \tag{1b}$$

that has been extended to make disturbances $d_k \in \mathbb{R}^{m_d}$ and their input matrix $B_d \in \mathbb{R}^{n\times m_d}$ explicit. For this study, d_k is the deviation in horizontal wind speed from the nominal operating condition. $x_k \in \mathbb{R}^n$, $u_k \in \mathbb{R}^m$, $y_k \in \mathbb{R}^p$, $A \in \mathbb{R}^{n\times n}$, $B \in \mathbb{R}^{n\times m}$, and $C \in \mathbb{R}^{p\times n}$ have their usual meanings in the discrete-time model.

The modeling methodology is described briefly here. We consider a first-order continuous time input-output model (Pao and Johnson, 2011) from the blade pitch and wind speed to rotor speed, constructed using a step-input system identification procedure on the nonlinear, higher-dimensional FAST model. The model is linearized about a wind speed of 7 m/s using a constant generator torque for above-rated operation and given a state-space realization. The trim condition for linearization is found by altering the blade pitch angle in FAST simulations until the steady-state rotor speed reaches its rated value (see Table 1, where the $_{\text{nom}}$ subscript denotes nominal operation).

Table 1. Above-rated trim condition

Wind speed v_{nom} [m/s]	7
Rotor speed $\Omega_{\text{rpm,nom}}$ [rpm]	480 (rated)
Generator torque $\tau_{\text{gen,nom}}$ [Nm]	2.8 (rated)
Blade pitch β_{nom} [°]	6.2

The model is then expanded to add a state that integrates the rotor speed error, so that integral control action may be performed (Franklin et al., 2019), and then discretized using a zero-order hold at the sampling rate $f_s = 100$ Hz. Finally, the resulting discrete-time state-space model is further augmented to include the blade pitch position as a state, with the *difference* in blade pitch replacing the blade pitch position as an input. This allows us to penalize the pitch rate, rather than the pitch position, in the quadratic cost function (see Section 3.1).

Using the notation conventions $\delta w_k \coloneqq w_k - w_{\text{nom}}$ (i.e., the deviation away from nominal operation) and $\Delta w_{k,k-1} \coloneqq w_k - w_{k-1}$ (i.e., the difference in w between two successive discrete-time steps) for any signal w, the final model has the form of (1), with $x_k = \begin{bmatrix}\delta\Omega_k & \int \delta\Omega_{\text{rpm},k} & \delta\beta_{k-1}\end{bmatrix}^\mathsf{T}$, $u_k = \Delta\beta_{k,k-1}$, $d_k = \delta v_k$, and $y_k = \begin{bmatrix}\delta\Omega_{\text{rpm},k} & \int \delta\Omega_{\text{rpm},k}\end{bmatrix}^\mathsf{T}$. Ω is the rotor speed in radians per second and Ω_{rpm} is the rotor speed in revolutions per minute ($\Omega_{\text{rpm}} = {}^{60}/_{2\pi} \times \Omega$). By $\int \delta\Omega_{\text{rpm},k}$ we mean $\int_0^{t_k} \delta\Omega_{\text{rpm}} dt$, the integral of the rotor speed deviation from the beginning of controller time until the current time $t_k = {}^{k}/_{f_s}$.

The model matrices for MoWiTO are then $(A, B, B_d, C) =$

$$\left(\begin{bmatrix}0.97 & 0 & -5.12\\ 0.09 & 1.00 & -0.25\\ 0 & 0 & 1.00\end{bmatrix}, \begin{bmatrix}-5.12\\ -0.25\\ 1.00\end{bmatrix}, \begin{bmatrix}0.36\\ 0.02\\ 0\end{bmatrix}, \begin{bmatrix}9.55 & 0 & 0\\ 0 & 1.00 & 0\end{bmatrix}\right).$$

To clarify, the third element of the state accumulates the blade pitch angle differences $\Delta\beta$ up until the *previous* time step. The full effect of the blade pitch deviation (away from nominal) is a result of the third column of A ($A_3 = B$) and B, since

$$\begin{aligned} A_3\delta\beta_{k-1} + B\Delta\beta_{k,k-1} &= B\left(\beta_{k-1} - \beta_{\text{nom}} + \beta_k - \beta_{k-1}\right) \\ &= B\delta\beta_k\,. \end{aligned}$$

3. CONTROL

As mentioned previously, this work focuses on above-rated wind turbine control. As such, the control goal is to regulate the rotor speed to its rated value. The control algorithm we propose is an extension of the linear-quadratic regulator (LQR) to include preview disturbance information (Section 3.1). Contrary to the majority of feedforward control laws that have already been tested for wind turbines (Scholbrock et al., 2013; Schlipf et al., 2014; Haizmann et al., 2015; Schlipf et al., 2015), our method uses an optimal formulation (Verwaal et al., 2015) and can be seen as a step towards physical testing of a blade pitch-actuated MPC for wind turbines. We consider LQR as our baseline controller for comparison (Section 3.2).

3.1 Linear-quadratic Regulator with Disturbance Preview

We define our control problem in a similar fashion to LQR, but include the impact of future disturbances in the problem. Ostensibly, we would like

to find a feedback/feedforward (FB/FF) control law $u_k = f(\hat{x}_k; d_k, d_{k+1}, d_{k+2}, ...)$ that solves the problem

$$\underset{y_i, x_i, u_i}{\text{minimize}} \sum_{i=0}^{\infty} y_i^\mathsf{T} L y_i + u_i^\mathsf{T} R u_i \tag{2a}$$

$$\text{subject to } x_{i+1} = Ax_i + Bu_i + B_d d_{k+i} \tag{2b}$$

$$y_i = Cx_i \tag{2c}$$

$$x_0 = \hat{x}_k \tag{2d}$$

where $L \geq 0$; $R > 0$; (A, B) is controllable; $\hat{x}_k$ is an estimate of the state at the current time; and d_{k+i} is the disturbance, assumed to be known, affecting the system at the ith future time step. k denotes the current time step in real time and i refers to future 'predicted' time steps. If $d_{k+i} = 0 \, \forall \, i = 0, 1, 2, ..., \infty$, the problem (2) reduces to the discrete-time LQR problem with the celebrated solution

$$u_k = -K_{\text{FB}} \hat{x}_k \tag{3}$$

with $K_{\text{FB}} = (B^\mathsf{T} P B + R)^{-1} B^\mathsf{T} P A$ and P the solution to the discrete-time algebraic Riccati equation

$$P = A^\mathsf{T} P A + C^\mathsf{T} L C - A^\mathsf{T} P B (B^\mathsf{T} P B + R)^{-1} B^\mathsf{T} P A. \tag{4}$$

In reality, the disturbance cannot be known for all future time; instead, we assume that it is only known over some finite N-step prediction horizon and set $d_{k+i} = 0 \, \forall \, i \geq N$. From MPC theory, we rewrite (2) as the finite-horizon problem (substituting (2c) into (2a))

$$\underset{x_i, u_i}{\text{minimize}} \sum_{i=0}^{N-1} \left\{ x_i^\mathsf{T} Q x_i + u_i^\mathsf{T} R u_i \right\} + x_N^\mathsf{T} P x_N \tag{5a}$$

$$\text{subject to } x_{i+1} = Ax_i + Bu_i + B_d d_{k+i} \tag{5b}$$

$$x_0 = \hat{x}_k \tag{5c}$$

where $Q = C^\mathsf{T} L C$. The terminal cost $x_N^\mathsf{T} P x_N$ is the cost associated with minimizing $\sum_{i=N}^{\infty} x_i^\mathsf{T} Q x_i + u_i^\mathsf{T} R u_i$ subject to the model (5b) with zero disturbances ($d_i \equiv 0$) (Rawlings, 2000).

Problem (5) is expressed in matrix-vector form as

$$\underset{\mathbf{x}, \mathbf{u}}{\text{minimize}} \; \mathbf{x}^\mathsf{T} \mathbf{Q} \mathbf{x} + \mathbf{u}^\mathsf{T} \mathbf{R} \mathbf{u} \tag{6a}$$

$$\text{subject to } \mathbf{x} = \mathbf{A}\hat{x}_k + \mathbf{B}\mathbf{u} + \mathbf{B}_d \mathbf{d} \tag{6b}$$

where $\mathbf{x} \coloneqq \begin{bmatrix} x_0^\mathsf{T} & x_1^\mathsf{T} & \cdots & x_N^\mathsf{T} \end{bmatrix}^\mathsf{T}$, $\mathbf{u} \coloneqq \begin{bmatrix} u_0^\mathsf{T} & u_1^\mathsf{T} & \cdots & u_{N-1}^\mathsf{T} \end{bmatrix}^\mathsf{T}$, and $\mathbf{d} \coloneqq \begin{bmatrix} d_k^\mathsf{T} & d_{k+1}^\mathsf{T} & \cdots & d_{k+N-1}^\mathsf{T} \end{bmatrix}^\mathsf{T}$;

$$\mathbf{A} \coloneqq \begin{bmatrix} I \\ A \\ A^2 \\ \vdots \\ A^N \end{bmatrix}, \; \mathbf{B} \coloneqq \begin{bmatrix} 0 & \cdots & 0 \\ B & 0 & \vdots \\ AB & B & \ddots \\ \vdots & & \ddots \; 0 \\ A^{N-1}B & A^{N-2}B & \cdots \; B \end{bmatrix},$$

and $\mathbf{B}_d$ is built in the same way as $\mathbf{B}$ with B_d replacing B. Finally, $\mathbf{Q} \coloneqq \text{blockdiag}\,(Q, \ldots, Q, P)$ and $\mathbf{R} \coloneqq \text{blockdiag}\,(R, \ldots, R)$ where blockdiag$(\cdot)$ is a block diagonal matrix with the arguments on the lead diagonal.

We condense the problem by substituting (6b) into (6a), thus eliminating the states $\mathbf{x}$ from the decision variable and arriving at the unconstrained problem

$$\underset{\mathbf{u}}{\text{minimize}} \; \mathbf{u}^\mathsf{T} \mathbf{H} \mathbf{u} + 2\mathbf{h}^\mathsf{T} \mathbf{u}\,, \tag{7}$$

where $\mathbf{H} = \mathbf{B}^\mathsf{T} \mathbf{Q} \mathbf{B} + \mathbf{R}$ and $\mathbf{h} = \mathbf{B}^\mathsf{T} \mathbf{Q} \begin{bmatrix} \mathbf{A} & \mathbf{B}_d \end{bmatrix} \begin{bmatrix} \hat{x}_k \\ \mathbf{d} \end{bmatrix}$. The closed-form solution to (7) is

$$\begin{aligned} \mathbf{u} &= -\mathbf{H}^{-1} \mathbf{h} \\ &= -\left(\mathbf{B}^\mathsf{T} \mathbf{Q} \mathbf{B} + \mathbf{R} \right)^{-1} \mathbf{B}^\mathsf{T} \mathbf{Q} \begin{bmatrix} \mathbf{A} & \mathbf{B}_d \end{bmatrix} \begin{bmatrix} \hat{x}_k \\ \mathbf{d} \end{bmatrix}. \end{aligned}$$

Taking the first (block) entry of $\mathbf{u}$ provides the control at the current time step, which we express as

$$u_k = \begin{bmatrix} -K_{\text{FB}} & K_{\text{FF}} \end{bmatrix} \begin{bmatrix} \hat{x}_k \\ \mathbf{d} \end{bmatrix}. \tag{8}$$

This controller is referred to as the feedback/feedforward (FB/FF) law.

We emphasize that K_{FB} from (8) is identical to that from (3), i.e. K_{FB} is the LQR gain. To see this, consider defining $\mathbf{g}_1 = \mathbf{B}^\mathsf{T} \mathbf{Q} \mathbf{A}$ and $\mathbf{g}_2 = \mathbf{B}^\mathsf{T} \mathbf{Q} \mathbf{B}_d$. Then $\mathbf{h} = \begin{bmatrix} \mathbf{g}_1 & \mathbf{g}_2 \end{bmatrix} \begin{bmatrix} \hat{x}_k \\ \mathbf{d} \end{bmatrix}$ and we can express (7) as

$$\underset{\mathbf{u}}{\text{minimize}} \; \mathbf{u}^\mathsf{T} \mathbf{H} \mathbf{u} + 2\hat{x}_k^\mathsf{T} \mathbf{g}_1^\mathsf{T} \mathbf{u} + 2\mathbf{d}^\mathsf{T} \mathbf{g}_2^\mathsf{T} \mathbf{u}\,. \tag{9}$$

Now, consider the case when $\mathbf{d} \equiv 0$. Problem (9) reduces to the LQR problem and the unique solution $\mathbf{u} = -\mathbf{H}^{-1} \mathbf{g}_1 \hat{x}_k$ is a vector of the LQR optimal u over N steps. Call this solution $\mathbf{u}^{(1)}$. In particular, the first block element of $\mathbf{u}^{(1)}$ is $u_k^{(1)} = -K_{\text{FB}} \hat{x}_k$.

Next, consider (9) when $\hat{x}_k \equiv 0$. This is the situation where state regulation has already been achieved but there are future disturbances. The unique optimal solution is now the (feedforward only) control sequence $\mathbf{u} = -\mathbf{H}^{-1} \mathbf{g}_2 \mathbf{d} \coloneqq \mathbf{u}^{(2)}$ and the first block element can be written as $u_k^{(2)} = K_{\text{FF}} \mathbf{d}$.

Finally, we have claimed that the optimal solution of (7) and (9) when $\mathbf{d} \not\equiv 0$ and $\hat{x}_k \not\equiv 0$ is $\mathbf{u} = \mathbf{u}^{(1)} + \mathbf{u}^{(2)}$. Since $\mathbf{u}^{(1)} + \mathbf{u}^{(2)}$ is the unique stationary point of the (positive definite) cost function (9), we see that the claim holds.

3.2 Feedback-only Controller

We use a feedback-only (FB only) control law as the baseline controller. The feedback controller is simply the LQR controller (3) found by solving problem (2) with disturbances set equal to zero. This ensures similarity between controllers, in that both are designed to minimize the cost function (2a).

3.3 State Estimation

Throughout the derivation of the FB/FF and FB only control laws, we have used $\hat{x}_k$ to denote the estimate of the state at the current time step. In general, an observer needs to be designed to estimate x based on y and u. In our case, $\hat{x}$ can be calculated directly because it depends only on the rotor speed Ω_{rpm}, which is measured, and the commanded blade pitch angle β. The calculated value $\hat{x}$ is still noisy, and we have still chosen to use the hat notation to differentiate it from the true state x of the system.

4. TEST SETUP

Experimental tests were carried out on MoWiTO operating in the wind tunnel facility at ForWind – Center for Wind Energy Research at the University of Oldenburg. The key elements of the test setup are described here and are shown schematically in Fig. 1.

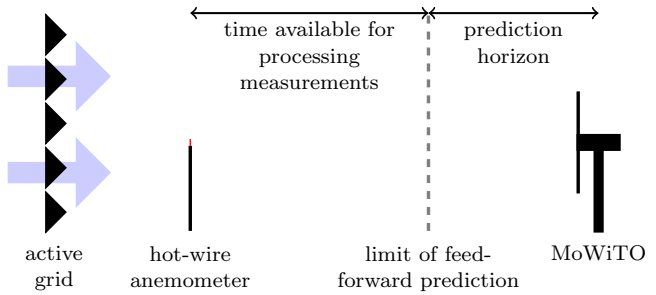

Fig. 1. Wind tunnel test setup. The active grid controls the airflow, the hot-wire anemometer measures wind speed, and the turbine control system responds to wind disturbances. The hot-wire measurements are filtered prior to use in the controller, and then advanced to account for the delay introduced by filtering.

4.1 Physical Layout

The ForWind Center's wind tunnel is a closed-circuit tunnel with a 3×3 m^2 cross-sectional open test section. At the entry to the test section, ForWind operates an 'active grid', which is capable of recreating complex turbulent wind structures by means of vanes that control the airflow (Kröger et al., 2018). MoWiTO is placed about 5 m downstream from the active grid. In most research for utility-scale turbines, lidars are used to generate the preview measurements for feedforward control. For this scaled study in a wind tunnel test bed, we replace the lidar with a hot-wire anemometer placed 1.5 rotor diameters (1.5D) upstream of the turbine.

4.2 Controller Implementation

Both the FB only and FB/FF controllers are implemented in a LabVIEW virtual instrument (VI) running on a CompactRIO. The VI allows toggling between the two controllers online and is embedded in a larger VI that includes spin-up and shut-down procedures for the turbine.

4.3 Preview Measurement Filter

For both lidars and hot-wire anemometers preview measurements require filtering, before they can be used by a feedforward controller, to remove noise at the sensor and high-frequency turbulence in the signal that evolves before reaching the turbine (Simley and Pao, 2015).

We use a moving average filter to process the preview measurements. To ensure that there is good alignment between the filtered preview data and the wind field, we advance the filter output by the (frequency independent) group delay of the filter (Sinner and Pao, 2019). The resulting noncausal filter has the transfer function

$$H(z) = \frac{1}{n_{\text{filt}}} \frac{z^{n_{\text{filt}}-1} + z^{n_{\text{filt}}-2} + \cdots + z + 1}{z^{(n_{\text{filt}}-1)/2}} \tag{10}$$

where n_{filt} is the number of samples in the moving average, and must be an odd positive integer. In order to implement the filter (with the advance), we leave some time between when the measurements are taken and when they are required by the FB/FF controller (8). The associated propagation range is sketched in Fig. 1.

There is a trade-off between the controller prediction horizon length N and the amount of filtering possible, represented by n_{filt}. The filter order is upper bounded as $n_{\text{filt}} \leq 2\lfloor {}^{\ell f_s}/_{v_{\text{nom}}} - N \rfloor + 1$ (Sinner and Pao, 2019) where $\ell = 2.7$ m is the upstream distance of the hot-wire relative to the turbine and $v_{\text{nom}} = 7$ m/s (Table 1). $\lfloor \cdot \rfloor$ represents the floor function, which rounds its argument down to the nearest integer. Due to hardware limitations, the controller update rate is set as $f_s = 100$ Hz. We then choose $N = 20$ and $n_{\text{filt}} = 35$, close to the maximum allowable ($n_{\text{filt}} = 37$). The filter is also implemented in LabVIEW.

5. RESULTS

5.1 Simulation Results

To verify and tune the operation of the controllers, both the FB only case and the FB/FF controller were tested in closed-loop simulations using the FAST Simulink interface (Jonkman and Buhl Jr., 2005). A simplified gust wind profile of mean wind speed 7 m/s with noise added was provided to both control systems (Fig. 2, top, black line). Further noise was added to the profile before passing it through the preview filter (10), resulting in the green line Fig. 2 (top). After some manual tuning to achieve 'reasonable' speed regulation without excessive blade pitching, the weighting matrices for the cost function (2a) were chosen as $L = I_2$ and $R = 1 \times 10^5$.

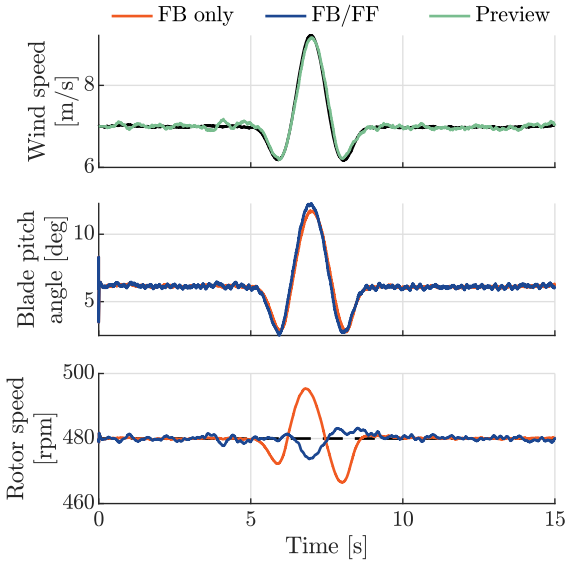

Fig. 2. Simulated controller behavior for a gust event. In the top plot, the black line represents the true wind seen by the turbine, while the green line represents the filtered hot-wire anemometer measurement of wind speed that the FB/FF controller uses as disturbance preview. The black dashed line in the bottom plot is the rated rotor speed $\Omega_{\text{rpm,nom}}$.

The lower two plots in Fig. 2 show the blade pitch and rotor speed responses with these weights, respectively. It is clear from the peak rotor speed response and slight phase lead in the pitch signal that the feedforward component is working as intended. The extra noise in the rotor speed signal under FB/FF control comes from the noisy pitch

signal, which in turn is a result of responding to a noisy disturbance preview signal (even after filtering). This is a shortcoming of the control system, but not something that we consider to be a major concern for full-scale wind turbines using lidars (rather than hot-wire anemometers) for preview (see end of Section 5.2 for discussion).

5.2 Experimental Results

During testing, the active grid provided ten gust events approximately 7 seconds apart in the otherwise uniform (nominally) 7 m/s airflow. The FB only controller was tested first, followed immediately by the FB/FF controller. A subset of the gusts and responses has been overlaid in Fig. 3 to emphasize differences.

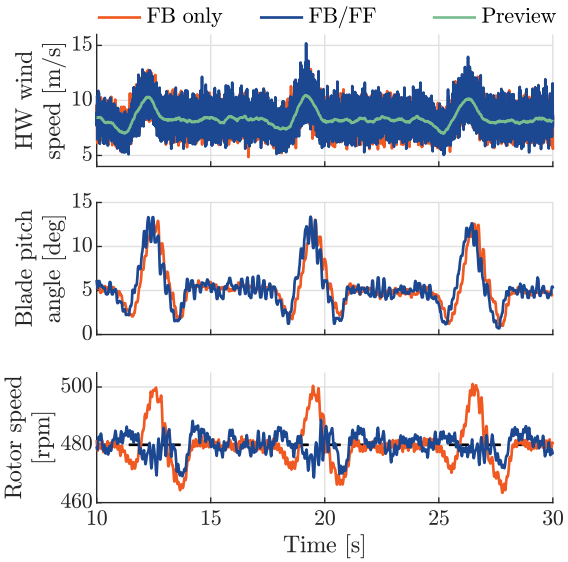

Fig. 3. Controller behavior for three gust events. In the top plot, the orange and blue lines represent hot-wire (HW) anemometer readings for the tests for each controller. The green preview measurement is a filtered version of the blue HW measurement used by the FB/FF controller. The orange HW measurement is not used by the controller, but is reproduced here to demonstrate similarity between the test conditions. The black dashed line in the bottom plot is the rated rotor speed $\Omega_{\text{rpm,nom}}$.

We see clearly the impact of feedforward control. The FB/FF controller is able to preempt the gust and starts pitching the blades earlier to maintain the rotor speed at rated. Although the FB only controller goes through almost the exact same pitch cycle, it is delayed because the effect of the gust on the rotor speed must be measured before counteraction is taken. This delay causes significantly more deviation from the rated rotor speed.

In fact, it appears that the feedforward controller is taking action too early, presumably due to an unaccounted-for slow-down effect as the wind approaches the turbine rotor (Dunne et al., 2014). This causes the rotor speed to drop further (and earlier) than expected, and leads to oscillations in the response following the initial drop. We have since recreated this effect in simulation (by advancing the preview measurement too far), but omit graphical results for brevity.

The effect of noisy preview measurements is also clear, especially in the time between gusts (e.g., 14–17 seconds). This signal noise is translated into noisier pitch actuation and finally poorer rotor speed regulation.

Statistics of the responses confirm the improvement of the FB/FF controller over the FB only controller for regulating rotor speed. In Table 2, the last column represents the percentage difference between the FB only and FB/FF controllers. Green (with a down arrow) represents a reduction (improvement), while red represents an increase (degradation), in the quantity of interest. We present standard deviation results for rotor speed and blade pitch both during gust events and between gust events to emphasize the noise injected by the preview measurements. We differentiate between peaks in rotor speed error as being positive (overspeeds) and negative (underspeeds), since there is a significant difference between these quantities (see Fig. 3).

Table 2. Controller test results

	FB only	FB/FF	Difference
Peak rotor speed deviation from rated (positive) [rpm]	21.2	10.1	▼52.6%
Peak rotor speed deviation from rated (negative) [rpm]	17.7	13.2	▼25.5%
Rotor speed standard deviation during gusts [rpm]	9.01	4.15	▼54.0%
Rotor speed standard deviation between gusts [rpm]	1.14	2.34	▲105%
Blade pitch standard deviation during gusts [°]	3.05	3.17	▲3.92%
Blade pitch standard deviation between gusts [°]	0.309	0.550	▲77.7%

It is apparent from the results presented here that the inclusion of the feedforward term in the control law can significantly improve rotor speed regulation. However, a more complete set of turbulent wind cases would be required to give conclusive results. We also note that there is some increase in pitch activity during the gust event, but we consider this a reasonable price to pay for the improvement in rotor speed regulation.

The data from in-between gusts is, at first glance, concerning. There is a considerable increase in pitch activity and, correspondingly, a severe increase in rotor speed variation. This is due to the noise injected by the hot-wire preview measurement, and as such, is more of an artifact of the present test setup and filtering than an inherent problem with the feedforward control law. On a utility-scale turbine using lidar there is more time available for filtering, as well as spatial filtering inherent to lidar operation, and we anticipate that the noise present in the feedforward signal would be lower than in this test. Overall, we consider the test results obtained to be in-line with simulated and field-tested feedforward controller results, further highlighting the benefits of feedforward action in wind turbine controls.

6. CONCLUSIONS AND FUTURE WORK

The experimental results presented in this work confirm the findings of others that wind preview measurements can

be useful for rotor speed regulation in above-rated winds. To the authors' knowledge, it is the first implementation of an optimal control technique using the feedforward extension for turbine blade pitch control.

The next step for this work is to also consider inequality constraints in the optimization problem (5). The inclusion of inequalities on the states and inputs would extend the present work to a model predictive control (MPC) problem whose solution cannot be expressed as a linear feedback/feedforward law. While several simulation studies have been published applying MPC to wind turbines (Schlipf et al., 2013; Lio et al., 2017; Sinner and Pao, 2019) with some emphasizing real-time capabilities (Bottasso et al., 2014; Gros and Schild, 2017), to our knowledge only one physical experiment has been conducted and was limited to generator torque control (Verwaal et al., 2015). Although solving the MPC problem at the controller sample rate is challenging, we believe that it is possible, and aim to extend our work to this problem in our continued investigation of preview-enabled MPC for wind turbines.

REFERENCES

F. Berger, L. Kröger, D. Onnen, V. Petrović, and M. Kühn. Scaled wind turbine setup in a turbulent wind tunnel. In *Jrnl. of Physics: Conf. Series*, volume 1104, 2018.

C.L. Bottasso, P. Pizzinelli, C.E.D. Riboldi, and L. Tasca. LiDAR-enabled model predictive control of wind turbines with real-time capabilities. *Renewable Energy*, 71, 2014.

F. Dunne, L.Y. Pao, A. Wright, B. Jonkman, and N. Kelley. Adding feedforward blade pitch control to standard feedback controllers for load mitigation in wind turbines. *Mechatronics*, 21(4), 2011.

F. Dunne, L.Y. Pao, D. Schlipf, and A.K. Scholbrock. Importance of lidar measurement timing accuracy for wind turbine control. In *Proc. American Control Conf.*, 2014.

G.F. Franklin, D.J. Powell, and A. Emami-Naeini. *Feedback Control of Dynamic Systems*. Pearson, 8th edition, 2019.

S. Gros and A. Schild. Real-time economic nonlinear model predictive control for wind turbine control. *Int. Jrnl. of Control*, 90(12), 2017.

F. Haizmann, D. Schlipf, S. Raach A. Scholbrock, A. Wright, C. Slinger, J. Medley, M. Harris, E. Bossanyi, and P.W. Cheng. Optimization of a feed-forward controller using a CW-lidar system on the CART3. In *Proc. American Control Conf.*, 2015.

M. Harris, M. Hand, and A. Wright. Lidar for turbine control. Technical Report NREL/TP-500-39154, NREL, 2005.

A. Jain, G. Schildbach, L. Fagiano, and M. Morari. On the design and tuning of linear model predictive control for wind turbines. *Renewable Energy*, 80, 2015.

B. Jonkman and J. Jonkman. FAST v8.16.00a-bjj. 2016. URL `wind.nrel.gov/nwtc/docs/README_FAST8.pdf`.

J. Jonkman, S. Butterfield, W. Musial, and G. Scott. Definition of a 5-MW reference wind turbine for offshore system development. Technical Report NREL/TP-500-38060, NREL, 2009.

J.M. Jonkman and M.L. Buhl Jr. FAST user's guide. Technical Report NREL/EL-500-38230, NREL, 2005.

L. Kröger, J. Frederik, J-W. van Wingerden, J. Peinke, and M. Hölling. Generation of user defined turbulent inflow conditions by an active grid for validation experiments. In *Jrnl. of Physics: Conf. Series*, volume 1037, 2018.

W.H. Lio, B.Ll. Jones, and J.A. Rossiter. Preview predictive control layer design based upon known wind turbine blade-pitch controllers. *Wind Energy*, 20(7), 2017.

M. Mirzaei and M.H. Hansen. A LIDAR-assisted model predictive controller added on a traditional wind turbine controller. In *Proc. American Control Conf*, 2016.

L.Y. Pao and K.E. Johnson. Control of wind turbines. *IEEE Control Systems Magazine*, 2011.

J.B. Rawlings. Tutorial overview of model predictive control. *IEEE Control Systems Magazine*, 20(3), 2000.

D. Schlipf and M. Kühn. Prospects of a collective pitch control by means of predictive disturbance compensation assisted by wind speed measurements. In *Proc. German Wind Energy Conf.*, 2008.

D. Schlipf, D.J. Schlipf, and M. Kühn. Nonlinear model predictive control of wind turbines using LIDAR. *Wind Energy*, 16(7), 2013.

D. Schlipf, P.A. Fleming, F. Haizmann, A. Scholbrock, M. Hofsäß, A. Wright, and P.W. Cheng. Field testing of feedforward collective pitch control on the CART2 using a nacelle-based lidar scanner. In *Jrnl. of Physics: Conf. Series*, volume 555, 2014.

D. Schlipf, P. Fleming, S. Raach, A. Scholbrock, F. Haizmann, R. Krishnamurthy, M. Boquet, and P.W. Cheng. An adaptive data processing technique for lidar-assisted control to bridge the gap between lidar systems and wind turbines. In *EWEA Conf. Proc.*, 2015.

A. Scholbrock, P. Fleming, L. Fingersh, A. Wright, D. Schlipf, F. Haizmann, and F. Belen. Field testing LIDAR based feed-forward controls on the NREL controls advanced research turbine. In *AIAA Aerospace Sciences Meeting*, 2013.

A. Scholbrock, P. Fleming, D. Schlipf, A. Wright, K. Johnson, and N. Wang. Lidar-enhanced wind turbine control: Past, present, and future. In *Proc. American Control Conference*, 2016.

E. Simley and L.Y. Pao. A longitudinal spatial coherence model for wind evolution based on large-eddy simulation. In *Proc. American Control Conf.*, 2015.

M.N. Sinner and L.Y. Pao. A study on horizon length for preview-enabled model predictive control of wind turbines. In *Proc. American Control Conf.*, 2019.

M.D. Spencer, K.A. Stol, C.P. Unsworth, J.E. Cater, and S.E. Norris. Model predictive control of a wind turbine using short-term wind field predictions. *Wind Energy*, 16(3), 2012.

N.W. Verwaal, G.J. van der Veen, and J-W. van Wingerden. Predictive control of an experimental wind turbine using preview wind speed measurements. *Wind Energy*, 18(3), Mar. 2015.